Research Article

Nano Research
2023, 16(5): 7248–7259

ISSN 1998-0124 CN 11-5974/O4
https://doi.org/10.1007/s12274-023-5374-3

Comparison of extruded cell nanovesicles and exosomes in their molecular cargos and regenerative potentials

Xianyun Wang[1,2,3,4,5,6], Shiqi Hu[5,6], Dashuai Zhu[5,6], Junlang Li[5,6], Ke Cheng[5,6] (✉), and Gang Liu[1,3,4] (✉)

[1] *Department of Cardiology, The First Hospital of Hebei Medical University, Shijiazhuang 050000, China*
[2] *Scientific Research Data Center, The First Hospital of Hebei Medical University, Shijiazhuang 050000, China*
[3] *Hebei Key Laboratory of Cardiac Injury Repair Mechanism Study, Shijiazhuang 050000, China*
[4] *Hebei International Joint Research Center for Structural Heart Disease, Shijiazhuang 050000, China*
[5] *Department of Molecular Biomedical Science, North Carolina State University, Raleigh 27607, North Carolina, USA*
[6] *Department of Biomedical Engineering, University of North Carolina, Chapel Hill and North Carolina State University, Raleigh 27607, North Carolina, USA*

Received: 2 August 2022 / **Revised:** 30 November 2022 / **Accepted:** 3 December 2022

ABSTRACT

Extracellular vesicles (EVs) generated from mesenchymal stem cells (MSCs) play an essential role in modulating cell–cell communication and tissue regeneration. The clinical translation of EVs is constrained by the poor yield of EVs. Extrusion has recently become an effective technique for producing a large scale of nanovesicles (NVs). In this study, we systematically compared MSC NVs (from extrusion) and EVs (from natural secretion). Proteomics and RNA sequencing data revealed that NVs resemble MSCs more closely than EVs. Additionally, microRNAs in NVs are related to cardiac repair, fibrosis repression, and angiogenesis. Lastly, intravenous delivery of MSC NVs improved heart repair and cardiac function in a mouse model of myocardial infarction.

KEYWORDS

nanovesicles (NVs), exosomes, cardiac repair, mesenchymal stem cells (MSCs), extracellular vesicles (EVs), myocardial infarction (MI)

1 Introduction

Mesenchymal stem cell (MSC) transplantation has attracted much attention in the treatment of myocardial infarction (MI) and other ischemic diseases. However, the bulk of systemically administered MSCs was trapped in the lung, then the liver, and ultimately the spleen, scarcely reaching the injured heart tissue [1–4]. Paracrine activities have been discovered to be the major regulatory mechanism for MSCs in regulating tissue healing. Extracellular vesicles (EVs) are crucial cell–cell communicators in the secretome of MSCs because they transmit biomolecules such as proteins, lipids, and non-coding RNA (miRNA, lnRNA, and cirRNA) to activate signaling pathways in target cells [5–9]. Injected EVs have been shown to support heart repair by preserving cardiac function, inhibiting fibrosis, promoting angiogenesis, and reducing inflammation [10–14]. However, a fundamental obstacle to clinical translation and mass production is the low yield of EVs or exosomes.

Recently, numerous methods for producing high-quality exosomes in large quantities have been reported [15]. The repeatable large-scale production of MSC exosomes from human adipose tissue using tangential flow filtration (TFF) has been proposed to treat acute kidney injury, albeit still requiring a lot of cells [16]. A nano-channel-based nanopore biochip technology could boost exosome synthesis more than 50 times [17]. Recent research has looked into the manufacturing of large-scale yield nanovesicles (NVs) utilizing a lipid extruder (LiposoFast LF-50, Avastin) [18]. This method can increase nanovesicle production by more than 11-fold. In a recent study, the viability and efficiency of macrophage-derived nanovesicles loaded with chemotherapeutic drugs were established [18, 19].

The similarities between EVs and NVs were initially identified in our earlier study, and the potential for cardiac healing in myocardial ischemia-reperfusion injury was systematically demonstrated [20]. However, the biological molecules and active ingredients of NVs and EVs were not completely compared. The fact that extruded NVs could activate mitogen-activated protein kinase (MAPK) signaling suggested that they contained bioactive cargo [18]. Using proteomics and RNA sequencing methods, we compared the cargos in NVs and EVs in this work. Finally, we looked into how cardiomyocytes internalized NVs. In a mouse model of myocardial infarction, we also compared the therapeutic potential of intravenous NVs and EVs.

2 Results

2.1 Morphology characterization and quantification of NVs

Cell-derived nanovesicles by extrusion have been characterized by cell membrane structure, while the source and nutrition

Address correspondence to Gang Liu, cardio2004@hebmu.edu.cn; Ke Cheng, ke_cheng@unc.edu

component have not been described. Therefore, we first prepared NVs following the schematic (Fig. 1(a)) and then analyzed the morphology, characterization, and quantification, comparing them with EVs. A more similar protein profiling between NVs and MSCs rather than EVs and MSCs was proven by sodium dodecyl sulfate-polyacrylamide gel electrophoresis (SDS-PAGE) (Fig. 1(b)).

Figures 1(c) and 1(d) indicated that NVs possessed 3.5× times the protein content and 4 times less RNA content than EVs based on the same number particles, respectively. Additionally, quality and quantity of extracted RNA measured by a micro-capillary electrophoresis system showed two clear peaks of ribosomal RNA (28 and 18 s) in the groups of NV and MSCs indicating the MSC source of NVs (Fig. 1(e)). But it is worth noting that small non-coding RNA (sncRNA) also exists in the NVs, implying a potential regulatory function. Lastly, the morphology analyses by transmission electron microscopy (TEM) and size distribution examination by nanoparticle tracking analysis (NTA) were completed, respectively. It is shown that NVs and EVs shared a similar lipid bilayer membrane structure, but NVs (~ 193 nm) were larger than EVs (~ 143 nm) (Figs. 1(f) and 1(g)). These results indicate that NVs are readily available nanocarriers to allow more access to produce drug-loaded nanovesicles for further application in various diseases.

2.2 Proteomics analysis of NVs

To identify the protein components, proteomics analysis of NVs was conducted to distinguish the main source of NVs. We tested the NV lysate for MSC organelle markers (GM130 for Golgi apparatus, calnexin for endoplasmic reticulum), and housekeeping proteins (glyceraldehyde-3-phosphate dehydrogenase (GAPDH) and β-actin). In the detection of organelle markers, MSCs and NVs had similar expression profiles, while exosomes had a lower expression level of these organelle proteins (Figs. 2(a) and 2(b)). The similarities in organelle-specific markers between NVs and MSCs indicated that the extruded nanovesicles kept the cytoplasmic and cytoskeletal components of the parent cells through the extrusion process. In order to detect and analyze the cytokine profile of NV cargoes, a proteome profiler cytokine array assay, incorporating 53 mouse angiogenesis-related proteins, was carried out to check for various cytokines. The results indicated that NVs and MSCs showed a more similar protein profiling, while exosomes displayed a greater abundance of cytokines than

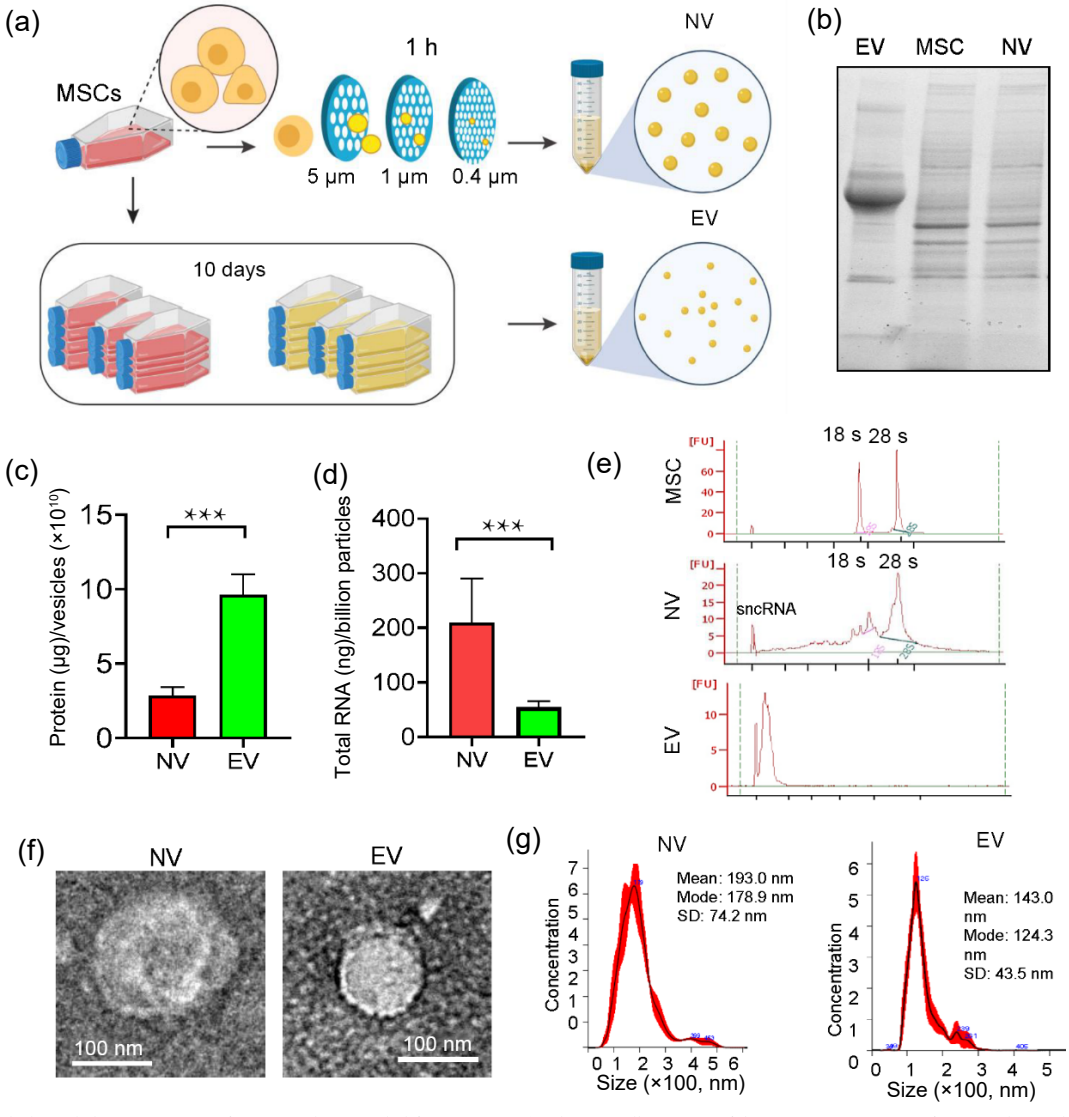

Figure 1 Morphological characterization of nanovesicles extruded from MSCs. (a) Schematic illustration of the generation process of NVs and EVs showing that EVs take more time and more flasks to manufacture. (b) Total protein profiles acquired through SDS-PAGE. The (c) protein and (d) RNA yields from one billion NVs or EVs. (e) A comparison of RNA distributions. (f) TEM images showing the particle size, structure (clear vesicles enclosed in a phospholipid bilayer), and spherical morphology of NVs and EVs. (g) Size distribution results indicated by NTA revealed that NVs (~ 193 nm) are larger, on average, than EVs (~ 143 nm). Data are presented as the mean ± SD of five independent biological samples. $^{*}P < 0.05$, $^{**}P < 0.01$, and $^{***}P < 0.001$.

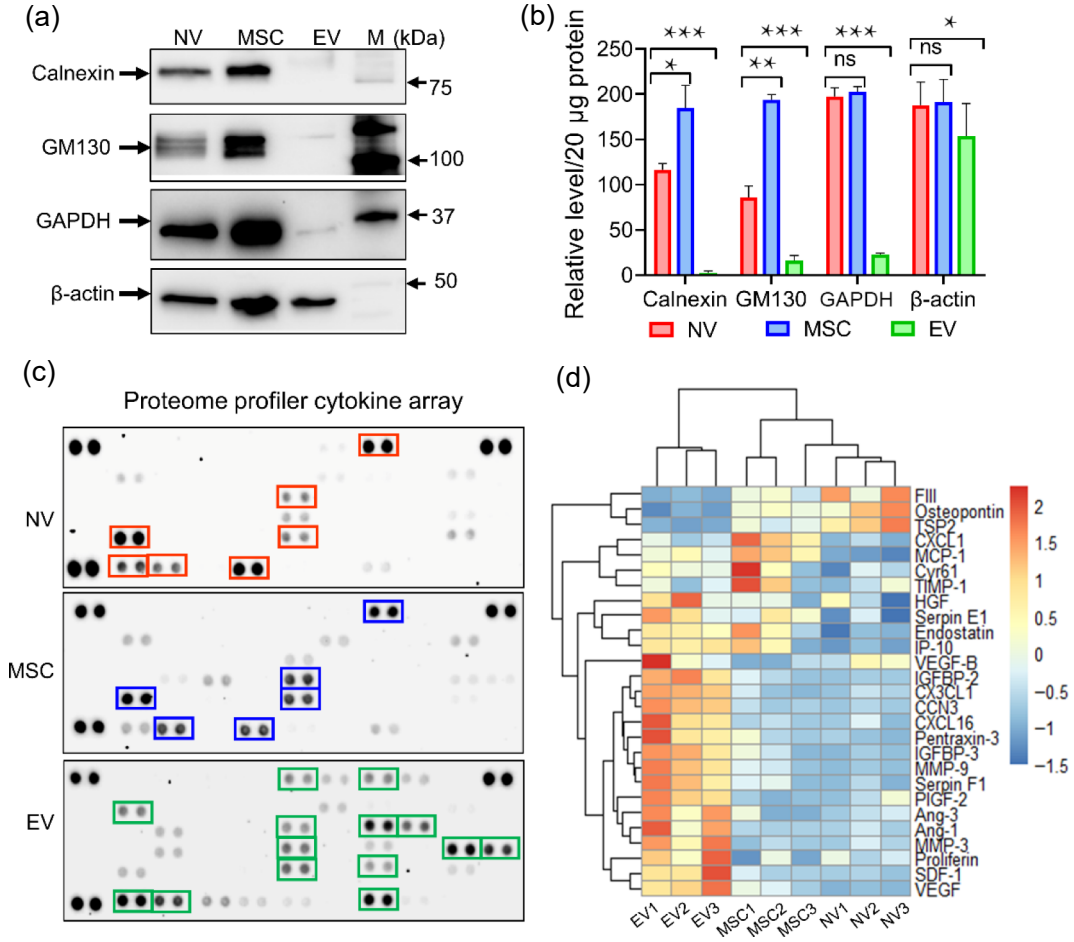

Figure 2 Comparative analysis of major protein components in NVs, EVs, and MSCs. (a) and (b) The expression levels of organelle proteins (GM130 for the Golgi apparatus and calnexin for the endoplasmic reticulum) and housekeeping proteins (GAPDH and β-actin) were analyzed by Western blotting. (c) Cytokine arrays, incorporating 53 proteins, showing the differences in cytokine profiles. (d) Distribution and expression abundance for the cytokines. Data are present as the mean ± SD of three independent biological samples. $^{*}P < 0.05$, $^{**}P < 0.01$, and $^{***}P < 0.001$.

MSCs and NVs (Figs. 2(c) and 2(d)). The position of proteins of interest in the proteome profiler cytokine array and the different expression levels in these groups are listed in Figs. S1(a) and S1(b) in the Electronic Supplementary Material (ESM), respectively. These results implied that NV proteins inherited from MSCs may not be the most crucial ingredients for the NVs' therapeutic effects. The similar expression profiles of organelles and constitutively expressed proteins between MSCs and NVs proved that NVs kept key cytoplasmic and cytoskeletal components from their parent cells.

To confirm whether exosomes were the major components of NVs, CD63-red fluorescent protein (RFP)-exosomes-green fluorescent protein (GFP)-MSCs were constructed, which can release CD63-RFP-exosomes (Fig. S2(a) in the ESM). We transferred the tetraspanin CD63-RFP cyto-Tracer into GFP-MSCs, and purified the population of cells that had taken up the RFP tracer successfully (Fig. S2(b) in the ESM). Successfully constructed CD63-RFP-exosomes-GFP-MSCs were amplified, and a small sample was analyzed with flow cytometry to confirm the dual expression of RFP and GFP. More than 90% of cells had dual expression (Fig. S2(c) in the ESM). In addition, attached cells with or without conditioned medium also indicated a successful constructed CD63-RFP-exosomes-GFP-MSCs (Fig. S2(d) in the ESM). Then, MSCs were stained with CM-DiD to label cytomembrane and were extruded through filter membranes of ever-decreasing pore sizes (5 μm, 1 μm, and 400 nm). The flow-through in every extrusion step was collected. The nuclear components of the flow-through were stained with 4',6-diamidino-2-phenylindole (DAPI) (Fig. S2(e) in the ESM). The different colors are due to different components: cell membrane (DiD, white), cytoplasm (GFP, green), exosomes (RFP, red), and nucleus (DAPI, blue). Fluorescence confocal microscopy showed that particles passing through the 5 and 1 μm filters lacked size uniformity. However, after being extruded through a 400 nm filter membrane, the resulting nanovesicles had a homogeneous size distribution (100–250 nm). Most of the NVs contained GFP-positive constituents and nuclei, but some nuclear fractions were not surrounded by a cell membrane, which was mainly due to the existence of an endomembrane system. Only a small fraction of exosomes appeared in the NVs (Fig. S2(e) in the ESM). Therefore, it was confirmed that the main cytoplasmic, nuclear, or genetic components were packaged into the NVs.

2.3 Comparative analysis of mRNA expression in NVs and EVs

To verify if mRNA exists in the NVs, the cell membrane was labeled with CM-DiD dye (purple), and mRNA was labeled with fluorescein isothiocyanate (FITC) (green). After the co-culture of NVs and human-derived cardiomyocytes (HuCMs) for 6 and 24 h, the green fluorescence intensity showed much stronger signals in the NV group than in the EV group (Figs. 3(a) and 3(b)), indicating the potential value of NVs for mRNA drug delivery [9, 21]. mRNA sequencing was further conducted to verify that the transcripts were intact rather than fragmented or damaged mRNA in the NVs (Figs. 3(c) and 3(d)). Heat map analysis of differently expressed transcripts indicated a similar

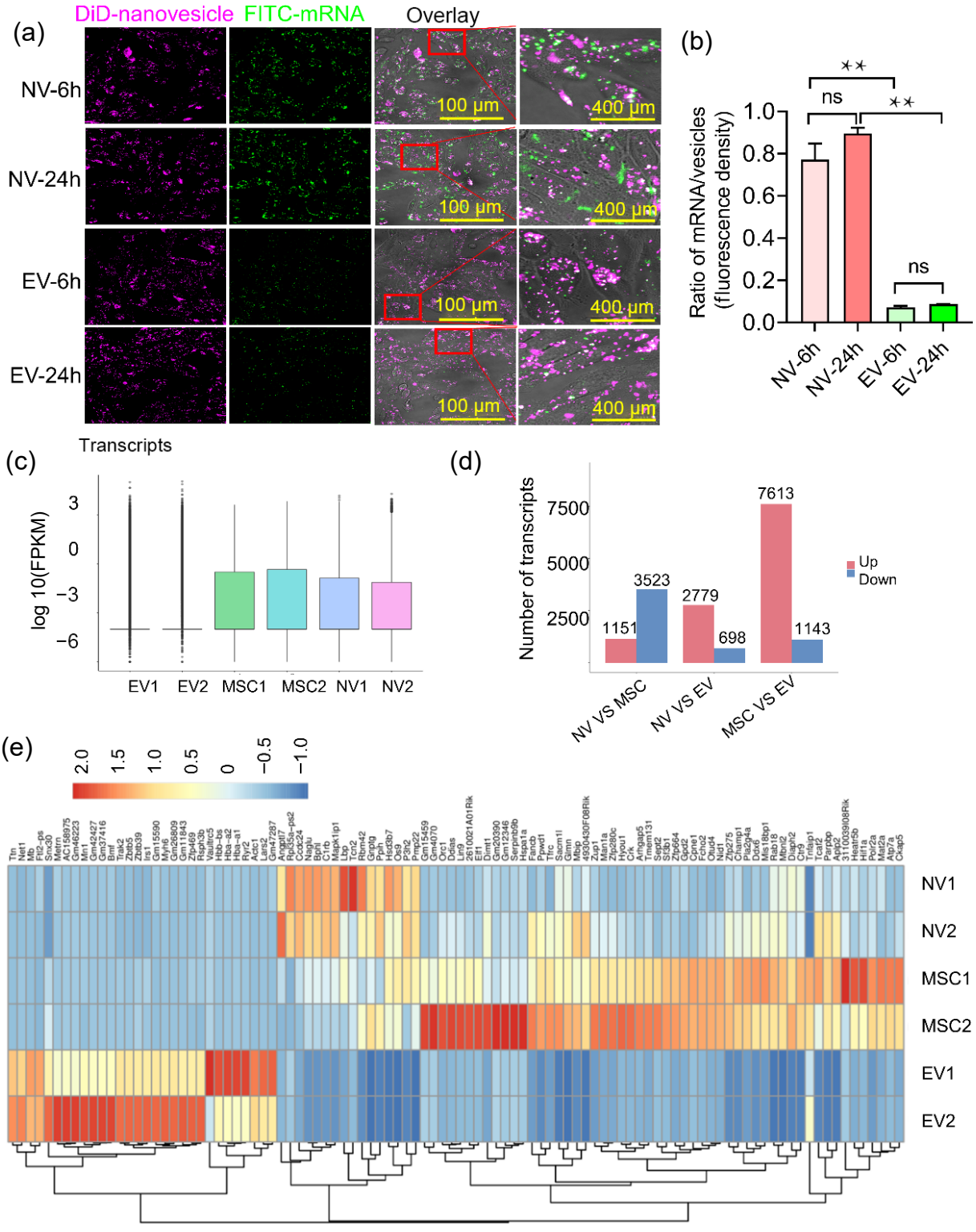

Figure 3 Comparison of mRNAs in NVs, MSCs, and EVs. (a) and (b) FITC tagged mRNA contents in DiD-labeled NVs or EVs were detected after coculture with HuCMs for 6 and 24 h. (c) Analysis of transcript content and (d) the number of differentially expressed transcripts. (e) Heatmap clustering analysis of the differential expressions of transcripts. Data are presented as the mean ± SD of three independent biological samples in (a). $^{*}P < 0.05$.

transcription profile between MSCs and NVs (Fig. 3(e)). Next, differential gene expression was displayed in heat map (Fig. S3 in the ESM). Together, the mRNA-seq data indicated that NV cargoes were directly derived from the parent cell components throughout the extrusion process. Although a small fraction of mRNA is packaged into EVs through exosome budding and releasing, mRNA is not the major content of exosomes. Therefore, this discovery may contribute to the design and production of therapeutic mRNA being delivered by NVs to treat various diseases.

2.4 MicroRNA sequencing analysis for NVs and EVs

Proteomics and mRNA-seq data have confirmed a high similarity between MSCs and NVs, while the components for exertion of function by NVs have not yet been demonstrated. Accumulating evidence has suggested that exosomes carry various cytokines and nucleic acids, including microRNAs, long noncoding RNA, and mRNA. All of these components help to regulate cell growth and biological metabolism [11, 22, 23]. Therefore, we investigated whether NVs contain noncoding RNAs. To further investigate the

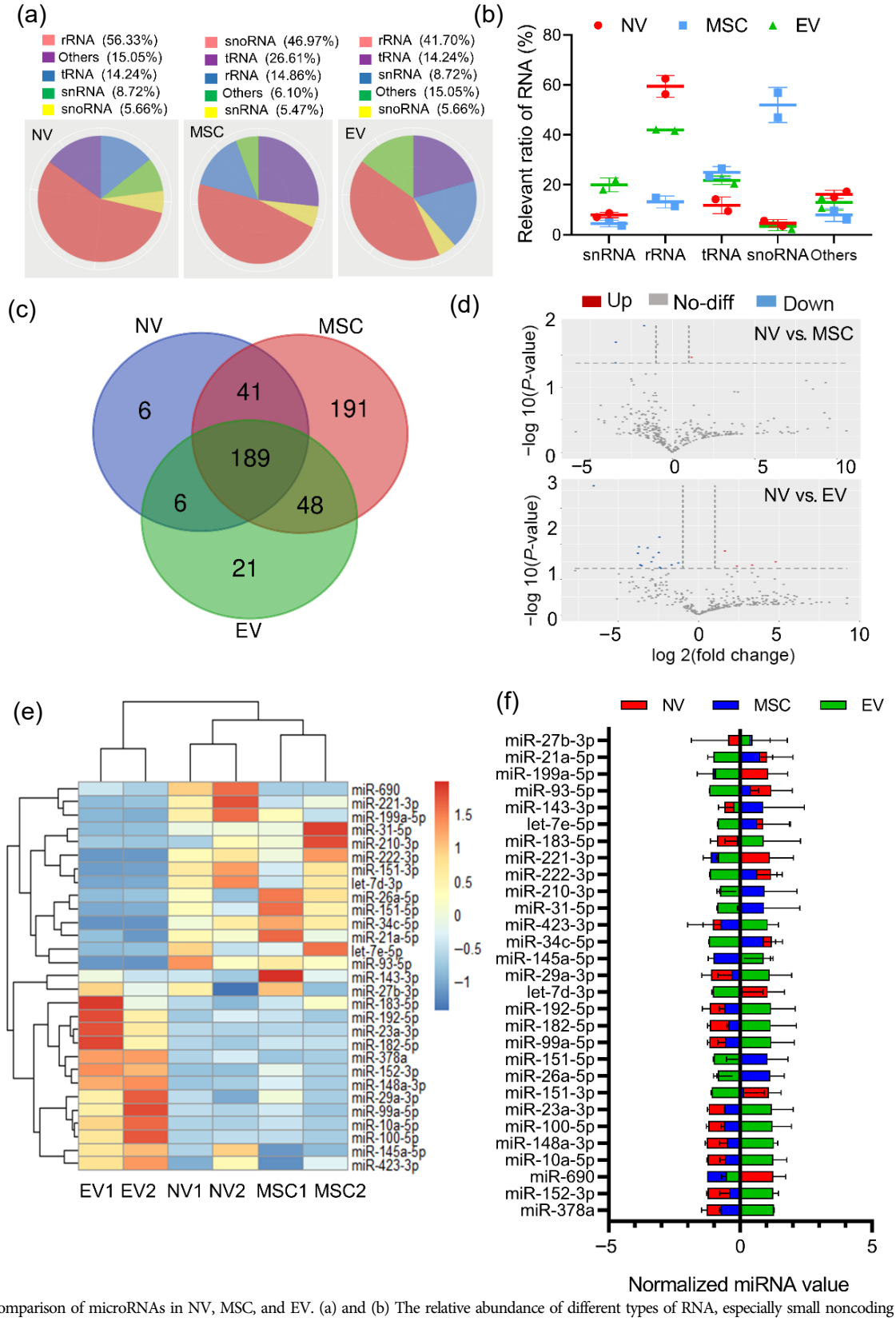

Figure 4 Comparison of microRNAs in NV, MSC, and EV. (a) and (b) The relative abundance of different types of RNA, especially small noncoding RNA, were displayed. The (c) Venn diagram and (d) the Volcano plot analysis of the differentially expressed microRNAs. (e) and (f) Heatmap clustering analysis of the differential expression of microRNAs. Each group's microRNA sequencing showed 2 distinct biological repeats. No-diff: no difference; rRNA: ribosome RNA; tRNA: transfer RNA; snRNA: small nuclear RNA; snoRNA: small nucleolar RNA.

differentially expressed miRNAs, miRNA sequencing was conducted on NV, EV, and MSC. miRNA expression profiles were analyzed and compared among the three groups (Figs. 4(a) and 4(b)). The Venn diagram of detected miRNAs is displayed in Fig. 4(c) and the differential expression characteristics are analyzed by volcano plot in Fig. 4(d). Additionally, the differentially expressed miRNAs were identified by heatmap (Figs. 4(e) and 4(f)), which showed that exosomes highly expressed some miRNAs such as miR-192-5p, miR-23a-3p, miR-182-5p, miR-148a-3p, miR-99a-5p, miR-10a-5p, and miR-100-5p. However, MSCs and NVs shared the highly similar expressed miRNAs. The miRNAs retained by NVs, like miR-690 (regulates mesenchymal

stem cell-induced angiogenesis), miR221-3p (promotes cell proliferation, is cardioprotective, and inhibits fibrosis), miR-31a-5p (promotes postnatal cardiomyocyte proliferation), miR-222 (induces cardiomyocyte growth and proliferation), Let-7d-3p (cardiac protection), and miR-93-5p (attenuates cardiac damage) were considered to be the major factors in cardiac protection after they were internalized by several heart cells. These results demonstrated that NVs contain a certain amount of noncoding RNA from their parent cells.

2.5 Internalization of NVs by cardiomyocytes

Due to the highly expressed miRNAs in the extruded NVs, internalization of the NVs by different types of cardiomyocytes was performed for further functional testing. Thus, the absorbing capacity of NVs by cardiomyocytes, including the H9C2 cell line and HuCM, was first evaluated by flow cytometry. We treated cardiomyocytes with NVs and EVs for 1, 3, and 6 h. Flow cytometry showed a higher internalization ratio of EVs than NVs at 1 h but quite an equal uptake level between NVs and EVs after 3 h (Figs. 5(a)–5(c)). How NVs were internalized by these cardiomyocytes was further verified by pretreating these cells for 1 h with diverse endocytosis blockers before adding NVs. The endocytosis inhibitors applied here were cytochalasin D (Cyto D, repressor of actin polymerization), chlorpromazine (CHL, targeting clathrin-mediated endocytosis), dynasore (DYN, inhibitor of dynamin), amiloride (AMI, targeting Na^+/H^+ pump related macropinocytosis), and filipin (FIL, inhibitor of cholesterol synthesis). Flow cytometry analysis (Figs. 5(d) and 5(e)) showed that DYN and Cyto D obviously inhibited the internalization ratio of NVs in both H9C2 and HuCM. These results demonstrated that NVs' internalization by cardiomyocytes mainly depends on dynamin and actin polymerization pathways.

2.6 Protective effects of NVs on oxidative stress-induced cardiomyocyte injury

The cardioprotective role of MSCs or MSC-exosomes against oxidative stress-induced myocardial cell apoptosis and reactive oxygen species (ROS) injury has been demonstrated in previous reports [24, 25]. Thus, we hypothesized that NVs derived from MSCs via extrusion might possess the effects of anti-apoptosis and anti-oxidative and anti-mitochondrial damage under hydrogen peroxide stimulation.

The generation of ROS is regarded as one of the most important causes of myocardial ischemia injury, and an oxidative stress injury model in cultured cardiomyocytes was established by treating cells with 50 μM tert-butyl hydrogen peroxide (TBHP) (ROS model) or 1 mM hydrogen peroxide (cell apoptotic model) for 4 h. Flow cytometry was conducted to analyze the levels of apoptotic cells, cellular ROS, and mitochondrial membrane potential. The results revealed that pretreatment with NVs or EVs for 3 h can significantly inhibit cell apoptosis (Figs. 6(a) and 6(b)), decrease ROS production (Figs. 6(c) and 6(d)), and reduce aggregate/monomer (A/M) ratios (Figs. 6(e) and 6(f)) in H9C2.

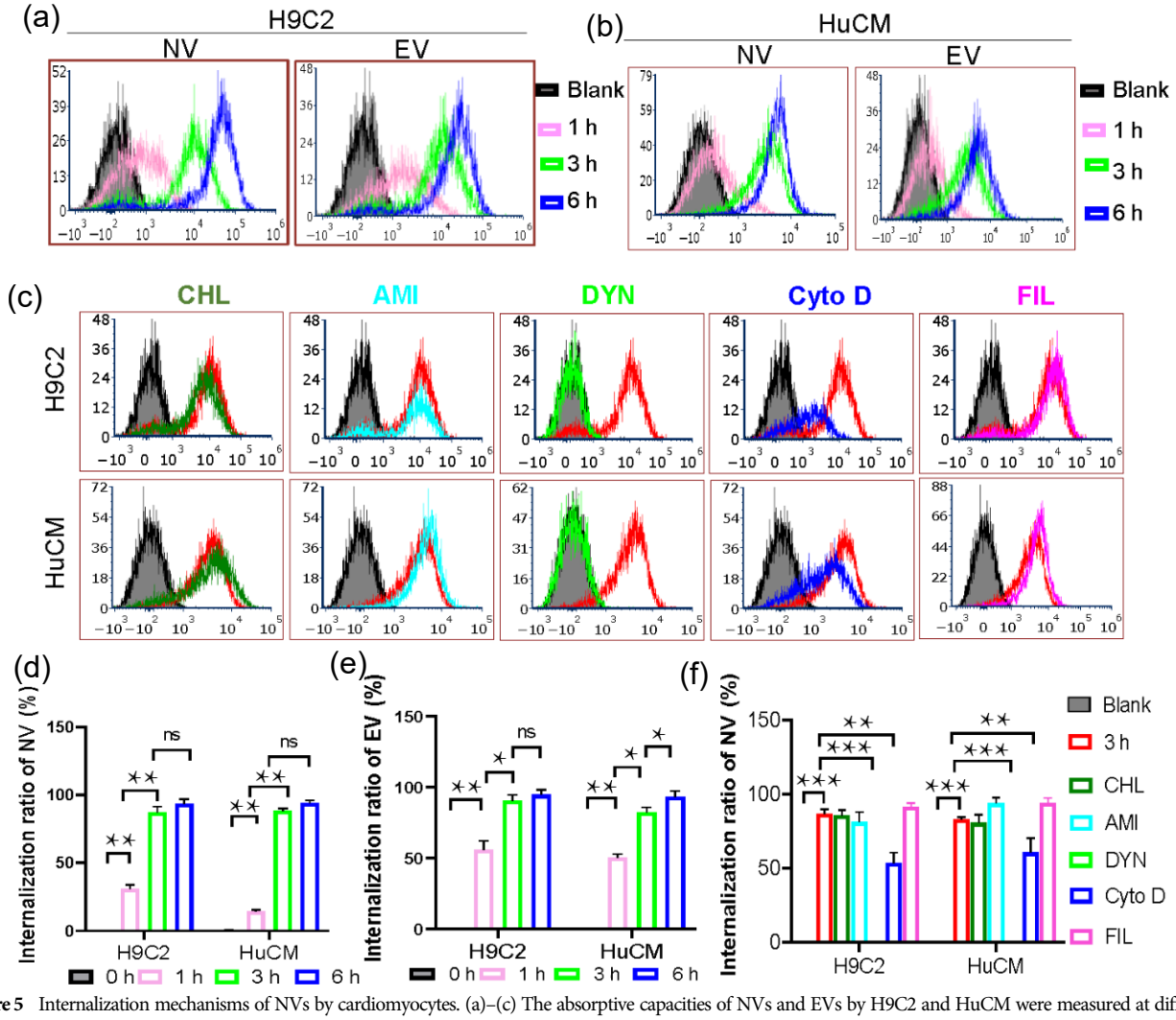

Figure 5 Internalization mechanisms of NVs by cardiomyocytes. (a)–(c) The absorptive capacities of NVs and EVs by H9C2 and HuCM were measured at different time periods (1, 3, and 6 h), respectively. (d) and (e) The molecular mechanisms of cellular internalization were evaluated by using different endocytosis inhibitors, including CHL, AMI, DYN, Cyto D, and FIL. Data are presented as the mean ± SD of three independent biological samples. *$P < 0.05$, **$P < 0.01$, and ***$P < 0.001$.

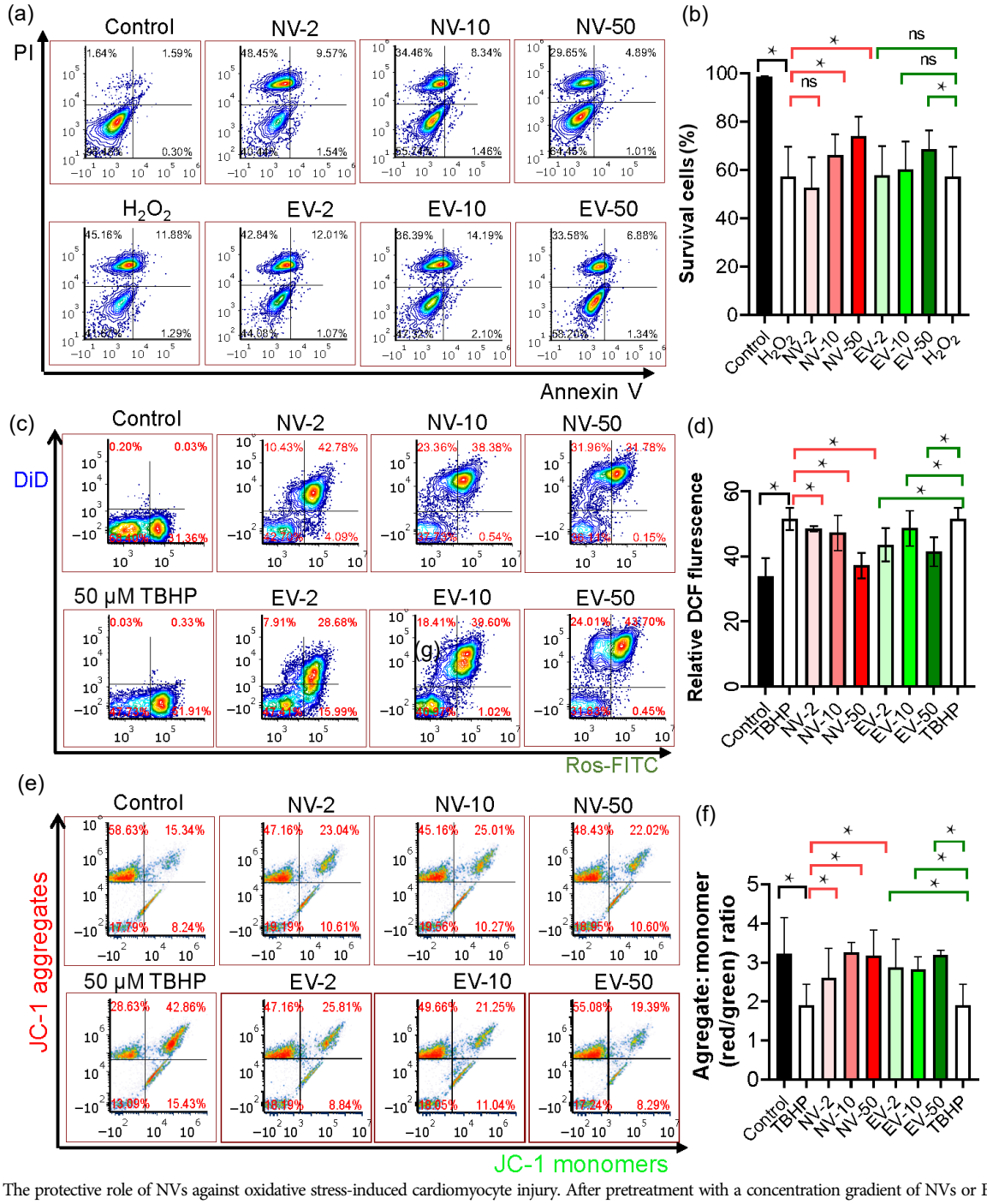

Figure 6 The protective role of NVs against oxidative stress-induced cardiomyocyte injury. After pretreatment with a concentration gradient of NVs or EVs (2, 10, 50 μg/μL) for 6 h, H9C2 were subjected to 50 μM TBHP or 1 mM hydrogen peroxide (cell apoptotic model) for 4 h. (a) and (b) Flow cytometry was performed to analyze survival cell ratio (Annexin V/PI double staining), cellular ROS level (dich lorofluorescin (DCF) fluorescence), and ((e) and (f)) mitochondrial membrane (tested by JC-1 assay) potential by counting A/M ratio. Data are presented as the mean ± SD of three independent biological samples. * $P < 0.05$.

Figures S4(a) and S4(b) in the ESM indicated a significant decrease in ROS level in HuCMs after being precultured with 10 or 50 μg/mL NVs for 3 h. 10 or 50 μg/mL NVs could also promote the proliferation of HuCMs after coculture for 48 h (Fig. S4(a) in the ESM). In summary, NVs can serve as a therapeutic agent to protect cardiomyocytes against oxidative stress-induced apoptosis, ROS generation, and mitochondrial damage and to promote cardiomyocyte proliferation.

2.7 Therapeutic benefits of NV infusion

In order to evaluate the cardiac protective effect of NVs in myocardial infarction, 20 μg NVs or EVs were intravenously administrated to mice with myocardial infarction. 28 days after treatment, cardiac function was evaluated by ultrasonic cardiogram (UC) and infarcted size was measured by Masson's trichome staining. Masson's trichrome staining showed significant decrease in infarcted size in both NV and EV groups compared to the meiosis I (MI) control group (Figs. 7(b) and 7(c)). The UC results (Fig. 7(d)) revealed a significant increase in left ventricular ejection fraction (LVEF, %) (Fig. 7(e)) and left ventricular fraction shortening (LVFS, %) (Fig. 7(f)), an obvious decrease of left ventricular end-diastolic volume (LVEDv, μL) (Fig. 7(g)), left ventricular end-systolic volume (LVESv, μL) (Fig. 7(h)), left ventricular end-diastolic dimension (LVEDd, mm) (Fig. 7(i)), and left ventricular end-systolic dimension (LVESd, mm) (Fig. 7(j)) both in the EV and NV group. However, there was no statistical significance between the NV and EV groups except for the LVESd. Additionally, the toxicity of NVs was tested by serum

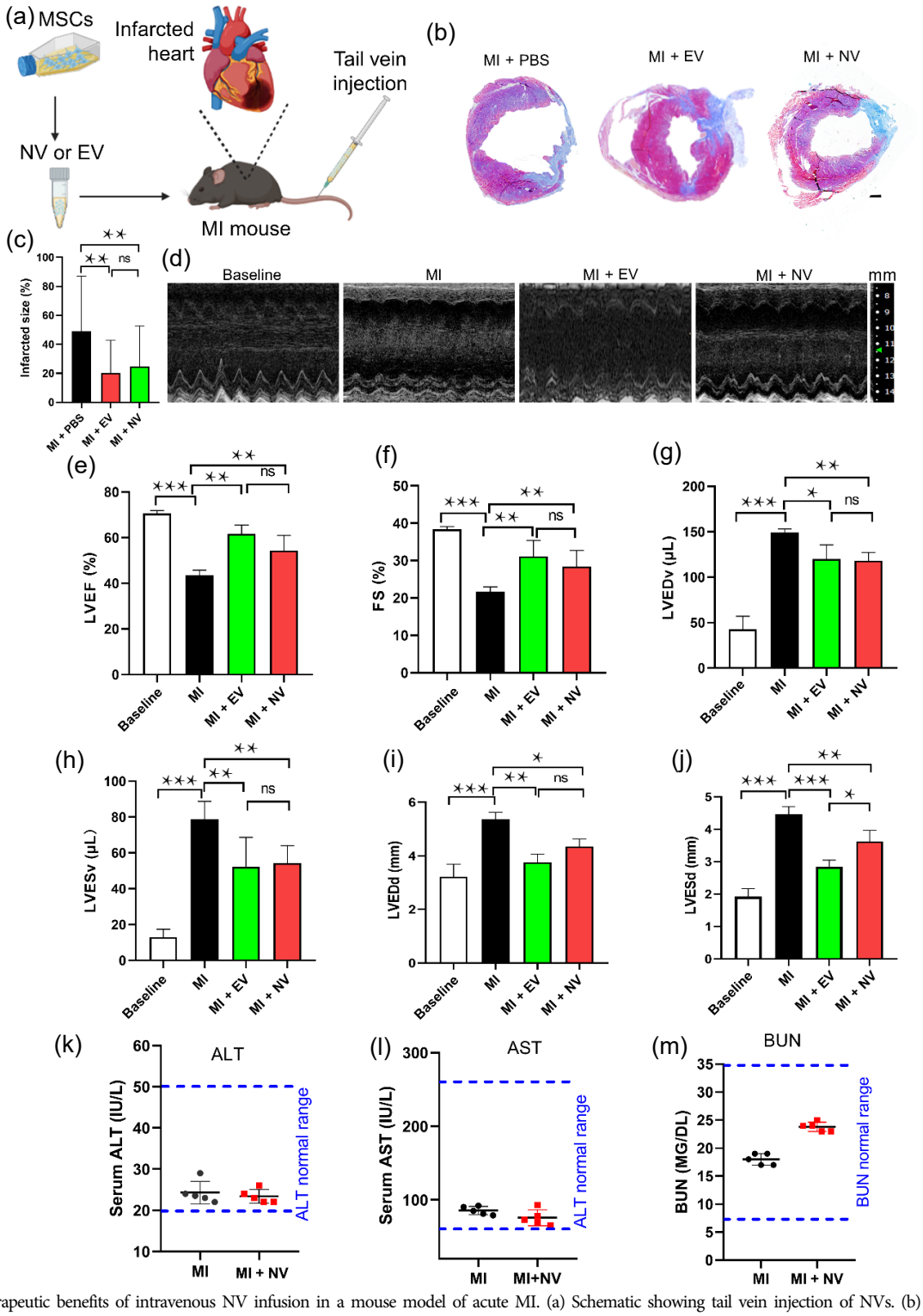

Figure 7 Therapeutic benefits of intravenous NV infusion in a mouse model of acute MI. (a) Schematic showing tail vein injection of NVs. (b) Representative Masson's trichrome staining images of control (PBS-treated MI mouse) and therapeutic groups (NVs-treated MI mouse, EVs-treated MI mouse) (Scale bar = 1 mm), and (c) the quantification of infarct sizes. (d) Representative long-axis echocardiography images were taken to evaluate the cardiac function improvement. (e) LVEF, (f) FS, (g) LVEDd, (h) LVESd, (i) LVEDv, and (j) LVESv were quantified respectively. The serum (k) ALT, (l) AST, and (m) BUN levels were respectively displayed. Data are presented as mean ± SD of 3–5 independent biological replicates. ns, no significance. * $P < 0.05$, ** $P < 0.01$.

alanine aminotransferase (ALT) (Fig. 7(k)), aspartate transaminase (AST) (Fig. 7(l)) (for liver functions), and blood urea nitrogen (BUN) (Fig. 7(m)) levels (for kidney functions), revealing no hepatic or renal function impairment after NV therapy. Therefore, the cardiac restoration mechanism of tail-injected NVs might be mainly attributed to the immunoregulation role of NVs which will be studied in our future research.

3 Discussion

MSCs have been broadly applied in basic and clinical research to benefit damaged heart, but the lack of efficacy and poor engraftment in the heart, and the concerns of tumorigenicity and immunological rejection severely limited further development and translation [26, 27]. MSC-derived exosomes have been considered the most crucial component for functional regulation of the injured heart through promoting cardiac preservation and angiogenesis, and inhibiting cardiac fibrosis and inflammation [28, 29]. However, the low yields, poor quality, and time consumption

of MSC exosome isolation severely limit the translational application of exosomes [19, 30]. To overcome these disadvantages, large-scaled nanovesicles with intracellular components achieved by extrusion were explored and the effective cargos and biological function were investigated in this research.

The NVs produced by cell extrusion through different nanopore-sized polycarbonate membranes are identified to have cell membrane structure by TEM imaging. which is consistent with the previous study [18, 31]. NV manufacturing by lipid extruder may produce more than 20 times as many NVs as EVs from similar amount of cells [21], which surpassed the approximately 2-fold yield of the previous study [18]. In addition, one cell can give rise to more than 2500 nanoparticles in less than 1 h, while EVs take several days from cell culture to isolation. The quantitative analysis of protein expression profile and RNA content in Fig. 1 confirmed more similarity between NVs and MSCs than between EVs and MSCs. The proteome profiler cytokine array (Fig. 2) and mRNA sequencing (Fig. 3) furtherly revealed that NVs inherited a certain amount of nutritional ingredients from the MSC parent. The manufacturing feasibility and high productivity, coupled with the stability and therapeutic efficacy of NVs, make them an ideal cell-free therapy candidate.

Up to now, although NVs produced by LF-50 have been shown to activate MAPK1/2-regulated kinase and have the ability to transfer mRNAs [18], the function of noncoding components, especially the microRNAs, was not clear. Exosomes have been proven to serve as "messengers" by delivering exosomal cargo including microRNAs, long noncoding RNA, mRNA, and also cytokines to target cells. After being internalized by recipient cells, the beneficial factors encapsulated in exosomes help to regulate tissue repair and biological metabolism [11, 23]. To determine the intracellular component in NVs responsible for the therapeutic efficacy, the proteome cytokine array test, mRNA, and microRNA sequencing were performed. Consistent with our assumptions, NVs inherited a large number of parent cell-derived protein and miRNAs.

The differentially expressed miRNAs revealed by miRNA sequencing provide important data support for further functional verification. The differently expressed miRNAs like miR-221, miR-222, let-7d-3p, and miR-93-5p have been disclosed via miRNA sequencing. It has been reported that miR-93-5p can protect H9C2 cells from hypoxia-induced cell injury by targeting inhibition of Atg7-mediated autophagy and TLR-4-mediated inflammatory response [32]. miR-221 showed cardio-protection through driving cardiomyocyte survival and inhibiting fibroblast activation to improve cardiac function and reduce cardiac remodeling post-MI [33]. miR-222 has also been found as a necessary factor for adult mammalian cardiomyocyte proliferation to restrain heart remodeling [34]. Overexpression of let-7d-3p could reduce cell apoptosis to promote cell survival by targeting HMGA2 under hypoxic conditions [35]. miR-93-5p was verified to suppress hypoxia-induced autophagy and inflammatory cytokine expression by targeting Atg7 and toll-like receptor 4 (TLR4) [32]. These functional miRNAs endow NVs to preserve cardiomyocytes through anti-apoptosis, oxidation resistance, and pro-proliferation as shown in this study (Fig. 4). Therefore, it is believed that the extrusion method will open a new therapeutic avenue to fight against heart damage induced by acute myocardial ischemia.

During the cell extrusion procedure, the lipid bilayer begins to self-assemble in an effort to stop the leakage of DNA and other components [36]. As shown in Fig. S1 in the ESM, the abundant DNA was packaged to NVs by extrusion, which was detected by DAPI staining. However, no proinflammatory effect of NVs was seen [20]. By utilizing this capability, we can create gene-based drugs for precision medicine in the future.

In order to verify the cardiac protection of NVs in MI, two cardiomyocyte cell lines (H9C2 and HuCM) were utilized to demonstrate the antioxidant stress and anti-apoptosis role of NVs. First, the internalization of NVs by cardiomyocytes was tested by flow cytometry which indicated that NVs could be effectively absorbed by H9C2 and HuCM, which will form an important basis for further functional verification *in vivo* [18].

However, there has been a lack of consensus on the internalization mechanisms and uptake selectivity of nanovesicles, which is dependent on a number of variables such as the source, size, and surface charge of the vesicles [37–39]. Although some studies suggested that all cell types can internalize EVs, others proved that recipient cells preferentially import EVs that originated from themselves [40, 41]. Additionally, recipient cells exhibit quicker absorption of EVs smaller than 100 nm [42] . Thus, NVs' early slower uptake could be due to their larger sizes. Future research is needed to examine the uptake selectivity and specificity of NVs to enhance their therapeutic application.

Next, cardiac preservation function of NVs against oxidative stress-induced cell apoptosis, ROS stress, and mitochondrial damage were studied (Fig. 6 and Fig. S4 in the ESM). Although the myocardial protective function has been provisionally confirmed, more research is still needed to fully understand the potential role of NVs' endosomal escape mechanism in enhancing therapeutic efficacy [43–45]. Future functional improvement can be achieved by designing pH-activated NVs with endosomal escape properties [44]. In addition, endosomal escape is not an issue when the uptake mechanism is cell-NV fusion instead of endocytosis. Therefore, these results primarily confirmed that NVs possess the ability to protect cardiomyocytes from myocardial ischemia injury, which provided important support for further functional verification in the MI model experiment.

To prove the repair effect of NVs in ischemia-induced myocardial injury, NVs were intravenously delivered through the tail vein. Four weeks after NV treatment, echocardiography revealed a clear rise in LVEF and FS (Fig. 7). Masson's trichrome staining, meanwhile, revealed a less infarcted size. These effects could be credited to the cardiac protection of NVs against oxidative stress-induced cell apoptosis, elevated ROS and mitochondrial membrane abnormalities (Fig. 6 and Fig. S4 in the ESM).

In conclusion, this study demonstrates that NVs inherit the main components necessary for MI repair from parent MSCs. Intact transcripts and many beneficial miRNAs were assigned to NVs after a series of extrusions. These extruded NVs had an important recovery effect in both *in vitro* and *in vivo* studies. Therefore, NVs present a crucial therapy option as a cell-free option replacing MSC treatment. Finally, the NVs can be optimized through cell membrane or cytoplasmic modifications via genetic overexpression or knock-down methods in parent cells. This extrusion production of NVs provides a robust manufacturing technique for larger yield and a more feasible strategy compared to EVs [46–48]. Therefore, a cell-free therapeutic strategy from extrusion-derived nanovesicles may act as an effective and feasible treatment method in the regenerative and translational medicine field.

4 Materials and methods

4.1 Cell lines

MSCs (Cyagen, MUXMX-90011), GFP-MSCs (Cyagen, MUBMX-01101), HuCMs (Celprogen, 36044-15), and H9C2 (Sigma-Aldrich, 88092904) were grown in Iscove's modified Dulbecco's

medium (IMDM) with 10% fetal bovine serum (FBS). The exosome Cyto-Tracer, pCT-CD63-RFP plasmid (System Bioscience, CYTO120RPA-1) was transfected to MSCs with GFP label using Lipofectamine™ 3000 (Invitrogen, L3000015), which were then subjected to flow sorting.

4.2 Myocardial infarction model

C57BL/6 mice (male, aged 8 weeks) were acquired from Jackson Laboratories. All animal studies were complied with the Laboratory Animal Care and Use Guide provided by the National Institutes of Health (NIH) as well as the Institutional Animal Care and Use Committee (IACUC) of North Carolina State University (approved No.: 19-811-B). Following intraperitoneal infusions of ketamine and xylazine to induce anesthesia, a myocardial infarction model was created by strangling the left anterior descending branch with a 6-0 Vicryl suture. Randomly, three groups of mice ($n \geq 5$) were divided: MI + phosphate buffered saline (PBS) group (200 μL PBS), MI + EV group (200 μL suspension with 20 μg EVs, equivalent to about $1 \subseteq 10^9$ particles produced by ~ $2 \subseteq 10^6$ cells for several days), and MI + NV group (200 μL suspension with 20 μg NVs, equivalent to about $5 \subseteq 10^9$ particles produced by ~ $2 \subseteq 10^5$ cells for several hours). At 4 weeks, heart function was monitored using an echocardiography, and the extent of the infarct was determined using Masson's trichrome staining.

4.3 Preparation of extrusion nanovesicles and exosomes

Adherent MSCs were collected after reaching 80% confluency and given three PBS buffer washes. Then, PBS was used to make a MSC suspension (2.5×10^6 cells/mL), and LiposoFast LF-50 (Avastin, York, UK) was used to push MSC suspension through a set of polycarbonate membranes with nanopore sizes (5, 1, and 0.4 μm) (Whatman). NVs were concentrated using a 100 kDa centrifugal filter unit at a 3500 g centrifugal force and subsequently filtered using a 0.22 μm syringe filter unit. Following that, morphology and biological characteristics were examined.

For exosome preparation, the cells were cultivated in IMDM basal medium for an additional three days after the MSC confluence reached about 80%. First, the conditioned medium was collected and pelleted using 5000 g of centrifugation for 5 min to remove cell debris and apoptotic bodies. For additional microvesicle removal, the supernatant was passed through a 220 nm filter. A 100 kDa ultra centrifugal filter was used to concentrate the EVs that included exosomes (Merck Millipore). For upcoming experiments, the morphology and biological characteristics were further examined.

4.4 Characterization of nanovesicles

TEM equipment was used to characterize the morphology of NVs and EVs after they had been negatively stained for 5 min after already being fixed with 2% paraformaldehyde and dried on a TEM grid. After being adjusted to the proper concentration, dynamic light scattering measurements (DLS) and NTA were used to analyze the size distribution of the NVs and EVs and the membrane zeta potential, respectively.

Then, total RNA quantification using NanoDrop One (ThermoFisher) and protein content determined by the BCA protein assay were carried out for the NV and EV groups. The protein profile was distinguished by SDS-PAGE and then captured by a Bio-Rad imaging system. To further determine the source of NVs, we employed western blotting to identify the levels of housekeeping proteins GAPDH (Invitrogen, Proteintech), β-actin (Invitrogen, MA5-15739), and organelle markers such as GM130 (NOVUS biologicals, NBP2-53420SS) for the Golgi apparatus and calnexin (Proteintech,10427-2-AP) for the endoplasmic reticulum. mRNA was labeled by the RNA Labeling kit (System Biosciences, EXOGR800A-1) following the manufacturer's instruction.

4.5 The protection role of NVs on myocardial cell line

Particularly after reperfusion, ROS generation in myocardial infarction can directly harm myocardial cells, leading to cell death or metabolic disorders. As a result, cell injury modeling of oxidant stress was created by stimulating H9C2 and HuCM with 50 μM TBHP or 500 μM hydrogen peroxide (H_2O_2) for 4 h. After cardiomyocyte pretreatment with different concentrations of NVs (2, 10, and 50 g/mL) or EVs (2, 10, and 50 g/mL) for 2 h, TBHP or H_2O_2 stimulation was subsequently performed for another 4 h. The A/M ratio measured by the JC-1 (Invitrogen, T3168) assay, the ROS level calculated by the cellular ROS assay kit (Abcam, ab113851), the anti-apoptotic role level analyzed by the annexin V-FITC/PI apoptosis kit, and the proliferation and toxicity evaluated by the cell counting kit-8 (CCK-8) measurement (Abcam, ab228554) at various time points were conducted, respectively.

4.6 Proteome profiler cytokine array assay

Following the manufacturer's instructions, the proteome profiler cytokine array (R&D system, ARY015) with 53 protein molecules was used to assess several cytokines. A mixture of biotinylated detection antibodies was added to 600–800 g of protein after 30 min of lysis on ice, and the mixture was then incubated overnight with a proteome profiler cytokine array. The loose material was subsequently removed by washing the membrane. The final step involved applying streptavidin-horseradish peroxidase (HRP) and chemiluminescent detection, which created a signal at each capture location corresponding to the amount of protein bound.

4.7 RNA sequencing

mRNA (poly(A) RNA based sequencing) and microRNA sequencing were completed by LC Sciences company. Heatmap clustering analysis showed the differentially expressed mRNA or miRNAs among the MSC, NV, and EV groups. The examination of the volcano plot showed the up- or down-regulated mRNAs or miRNAs (represented by red and blue plots, respectively).

4.8 Cardiac function assessment

Each mouse was subjected to transthoracic echocardiography evaluation of heart function while under isoflurane anesthesia on Day 0 (baseline), Day 7, and Day 8 post the MI modeling, respectively. Three measurements for each were taken. Researchers who were blinded to the animal and group identities examined LVEF, FS, LVEDd, LVESd, LVEDv, and LVESv.

4.9 Internalization and the mechanism analysis of NVs

The absorbing capacity of NVs by H9C2 and HuCM was evaluated using flow cytometry. Cells were taken to analyze the DiD fluorescence signal using flow cytometry after the CM-DiD-tagged NVs and these cells were cocultured for various time periods (1, 3, and 6 h). How NVs were internalized by these cardiomyocytes was further investigated using a variety of endocytosis inhibitors, such as 50 mg/mL CHL, 50 mg/mL DYN, 100 mg/mL AMI, 1 μM FIL, and 10 mg/mL Cyto D. After pretreatment with these inhibitors for 1 h, NVs were added for an additional 3 h period of co-culture. Finally, the CM-DiD positive cells were collected and analyzed using flow cytometry..

4.10 Statistical analysis

At least three times of each experiment were carried out

separately. Statistical analysis was performed using the GraphPad Prism program (GraphPad Software). All information is displayed as mean standard deviation (SD). For all comparisons between two groups, the two-tailed, unpaired student's *t*-test was used to assess the results. In order to compare more than two groups, one ANOVA analysis with post hoc Bonferroni correction was used. Differences were considered statistically significant when $P < 0.05$.

Acknowledgements

The funding for this study was provided in part by NC State University, the National Natural Science Foundation of China (No. 82200276), the Grant of Key Research and Development Program of Hebei Province (No. 203777117D), the Key Project of Hebei Provincial Health Commission (Nos. 20201159 and 20180224), the Natural Science Foundation of Hebei Province (Nos. H2021206399 and H2022206295). The overall experiments were designed by X. Y. W. The experiments and data analysis were done by X. Y. W, S. Q. H., J. L. L., and D. H. Z. The article was written by X. Y. W., K. C., and G. L. The final manuscript does have approval of all authors. Each author has given written permission to be listed as an author in the article by the corresponding author. The study's design, data collection, analysis, and interpretation, and the preparation of the manuscript were all done independently of the sponsoring organizations. BioRender was used to make the illustrations.

Electronic Supplementary Material: Supplementary material (Figs. S1–S4) is available in the online version of this article at https://doi.org/10.1007/s12274-023-5374-3.

References

[1] Harting, M. T.; Jimenez, F.; Cox. Jr. C. S. The pulmonary first-pass effect, xenotransplantation and translation to clinical trials—A commentary. *Brain* **2008**, *131*, e100.

[2] Fischer, U. M.; Harting, M. T.; Jimenez, F.; Monzon-Posadas, W. O.; Xue, H.; Savitz, S. I.; Laine, G. A.; Cox. Jr. C. S. Pulmonary passage is a major obstacle for intravenous stem cell delivery: The pulmonary first-pass effect. *Stem Cells Dev.* **2009**, *18*, 683–692.

[3] Leibacher, J.; Henschler, R. Biodistribution. migration and homing of systemically applied mesenchymal stem/stromal cells. *Stem Cell Res. Ther.* **2016**, *7*, 7.

[4] Barbash, I. M.; Chouraqui, P.; Baron, J.; Feinberg, M. S.; Etzion, S.; Tessone, A.; Miller, L.; Guetta, E.; Zipori, D.; Kedes, L. H. et al. Systemic delivery of bone marrow-derived mesenchymal stem cells to the infarcted myocardium: Feasibility, cell migration, and body distribution. *Circulation* **2003**, *108*, 863–868.

[5] Adamiak, M.; Sahoo. S. Exosomes in myocardial repair: Advances and challenges in the development of next-generation therapeutics. *Mol. Ther.* **2018**, *26*, 1635–1643.

[6] Balbi, C.; Vassalli. G. Exosomes: Beyond stem cells for cardiac protection and repair. *Stem Cells* **2020**, *38*, 1387–1399.

[7] Wang, Y. L.; Xie, W. P.; Liu, B.; Huang, H.; Luo, W.; Zhang, Y.; Pan, X. B.; Yu, X. Y.; Shen, Z. Y.; Li. Y. X. Stem cell-derived exosomes repair ischemic muscle injury by inhibiting the tumor suppressor Rb1-mediated NLRP3 inflammasome pathway. *Signal Transduct. Target. Ther.* **2021**, *6*, 121.

[8] Wang, X. Y.; Tang, Y. D.; Liu, Z.; Yin, Y. J.; Li, Q. H.; Liu, G.; Yan. B. Y. The application potential and advance of mesenchymal stem cell-derived exosomes in myocardial infarction. *Stem Cells Int.* **2021**, *2021*, 5579904.

[9] Popowski, K. D.; de Juan Abad, B. L.; George, A.; Silkstone, D.; Belcher, E.; Chung, J.; Ghodsi, A.; Lutz, H.; Davenport, J.; Flanagan, M. et al. Inhalable exosomes outperform liposomes as mRNA and protein drug carriers to the lung. *Extracell. Vesicle* **2022**, *1*, 100002.

[10] Wang, X.; Zhu, Y. H.; Wu, C. C.; Liu, W. N.; He, Y. J.; Yang. Q. Adipose-derived mesenchymal stem cells-derived exosomes carry microRNA-671 to alleviate myocardial infarction through inactivating the TGFBR2/Smad2 axis. *Inflammation* **2021**, *44*, 1815–1830.

[11] Mathiyalagan, P.; Sahoo, S. Exosomes-based gene therapy for microRNA delivery. In *Cardiac Gene Therapy*. Ishikawa, K. , Ed.; Humana Press: New York, 2017; pp 139–152.

[12] Qiao, L.; Hu, S. Q.; Liu, S. Y.; Zhang, H.; Ma, H.; Huang, K.; Li, Z. H.; Su, T.; Vandergriff, A.; Tang, J. N. et al. MicroRNA-21-5p dysregulation in exosomes derived from heart failure patients impairs regenerative potential. *J. Clin. Invest.* **2019**, *129*, 2237–2250.

[13] Zhu, D. S.; Liu, S.; Huang, K.; Wang, Z. Z.; Hu, S. Q.; Li, J. L.; Li, Z. H.; Cheng. K. Intrapericardial exosome therapy dampens cardiac injury via activating Foxo3. *Circ. Res.* **2022**, *131*, e135–e150.

[14] Vaka, R.; Van Remortel, S.; Ly, V.; Davis. D. R. Extracellular vesicle therapy for non-ischemic heart failure: A systematic review of preclinical studies. *Extracell. Vesicle* **2022**, *1*, 100009.

[15] Debbi, L.; Guo, S. W.; Safina, D.; Levenberg. S. Boosting extracellular vesicle secretion. *Biotechnol. Adv.* **2022**, *59*, 107983.

[16] Lee, J. H.; Ha, D. H.; Go, H. K.; Youn, J.; Kim, H. K.; Jin, R. C.; Miller, R. B.; Kim, D. H.; Cho, B. S.; Yi, Y. W. Reproducible large-scale isolation of exosomes from adipose tissue-derived mesenchymal stem/stromal cells and their application in acute kidney injury. *Int. J. Mol. Sci.* **2020**, *21*, 4774.

[17] Z. Q.; Shi, J. F.; Xie, J.; Wang, Y. F.; Sun, J. Y.; Liu, T. Z.; Zhao, Y. R.; Zhao, X. T.; Wang, X. M.; Ma, Y. F. et al. Large-scale generation of functional mRNA-encapsulating exosomes via cellular nanoporation. *Nat. Biomed. Eng.* **2020**, *4*, 69–83.

[18] Ilahibaks, N. F.; Lei, Z. Y.; Mol, E. A.; Deshantri, A. K.; Jiang, L. L.; Schiffelers, R. M.; Vader, P.; Sluijter. J. P. G. Biofabrication of cell-derived nanovesicles: A potential alternative to extracellular vesicles for regenerative medicine. *Cells* **2019**, *8*, 1509.

[19] Jang, S. C.; Kim, O. Y.; Yoon, C. M.; Choi, D. S.; Roh, T. Y.; Park, J.; Nilsson, J.; Lötvall, J.; Kim, Y. K.; Gho. Y. S. Bioinspired exosome-mimetic nanovesicles for targeted delivery of chemotherapeutics to malignant tumors. *ACS Nano* **2013**, *7*, 7698–7710.

[20] Wang, X. Y.; Hu, S. Q.; Li, J. L.; Zhu, D. S.; Wang, Z. Z.; Cores, J.; Cheng, K.; Liu, G.; Huang, K. Extruded mesenchymal stem cell nanovesicles are equally potent to natural extracellular vesicles in cardiac repair. *ACS Appl. Mater. Interfaces* **2021**, *13*, 55767–55779.

[21] Popowski, K. D.; Moatti, A. ; Scull, G.; Silkstone, D.; Lutz, H. ; de Juan Abad, B. L.; George, A.; Belcher, E.; Zhu, D. S.; Mei, X. et al. Inhalable dry powder mRNA vaccines based on extracellular vesicles. *Matter* **2022**, *5*, 2960–2974.

[22] Wen, Y.; Fu, Q.; Soliwoda, A.; Zhang, S.; Zheng, M. F.; Mao, W. J.; Wan. Y. Cell-derived nanovesicles prepared by membrane extrusion are good substitutes for natural extracellular vesicles. *Extracell. Vesicle* **2022**, *1*, 100004.

[23] Skotland, T.; Sandvig, K.; Llorente. A. Lipids in exosomes: Current knowledge and the way forward. *Prog. Lipid Res.* **2017**, *66*, 30–41.

[24] Arslan, F.; Lai, R. C.; Smeets, M. B.; Akeroyd, L.; Choo, A.; Aguor, E. N. E.; Timmers, L.; van Rijen, H. V.; Doevendans, P. A.; Pasterkamp, G. et al. Mesenchymal stem cell-derived exosomes increase ATP levels, decrease oxidative stress and activate PI3K/Akt pathway to enhance myocardial viability and prevent adverse remodeling after myocardial ischemia/reperfusion injury. *Stem Cell Res.* **2013**, *10*, 301–312.

[25] Liu, Z.; Xu, Y. Q.; Wan, Y. G.; Gao, J.; Chu, Y. Y.; Li. J. Exosomes from adipose-derived mesenchymal stem cells prevent cardiomyocyte apoptosis induced by oxidative stress. *Cell Death Discov.* **2019**, *5*, 79.

[26] Zhou, T.; Yuan, Z. N.; Weng, J. Y.; Pei, D. Q.; Du, X.; He, C.; Lai. P. L. Challenges and advances in clinical applications of mesenchymal stromal cells. *J. Hematol. Oncol.* **2021**, *14*, 24.

[27] Brown, C.; McKee, C.; Bakshi, S.; Walker, K.; Hakman, E.; Halassy, S.; Svinarich, D.; Dodds, R.; Govind, C. K.; Chaudhry. G. R. Mesenchymal stem cells: Cell therapy and regeneration potential. *J. Tissue Eng. Regen. Med.* **2019**, *13*, 1738–1755.

[28] Allan, D.; Tieu, A.; Lalu, M.; Burger. D. Mesenchymal stromal cell-derived extracellular vesicles for regenerative therapy and immune

modulation: Progress and challenges toward clinical application. *Stem Cells Transl. Med.* **2020**, *9*, 39–46.
[29] Khan, M.; Kishore, R. Stem cell exosomes: Cell-freetherapy for organ repair. In *Adult Stem Cells*. Di Nardo, P.; Dhingra, S.; Singla, D. K. , Eds.; Humana Press: New York, 2017; pp 315–321.
[30] Martin-Rendon, E.; Brunskill, S. J.; Hyde, C. J.; Stanworth, S. J.; Mathur, A.; Watt. S. M. Autologous bone marrow stem cells to treat acute myocardial infarction: A systematic review. *Eur. Heart J.* **2008**, *29*, 1807–1818.
[31] Cheng, G.; Li, W. Q.; Ha, L.; Han, X. H.; Hao, S. J.; Wan, Y.; Wang, Z. Q.; Dong, F. P.; Zou, X.; Mao, Y. W. et al. Self-assembly of extracellular vesicle-like metal-organic framework nanoparticles for protection and intracellular delivery of biofunctional proteins. *J. Am. Chem. Soc.* **2018**, *140*, 7282–7291.
[32] Liu, J. W.; Jiang, M.; Deng, S. Q.; Lu, J. D.; Huang, H.; Zhang, Y.; Gong, P. H.; Shen, X. M.; Ruan, H. J.; Jin, M. M. et al. MiR-93-5p-containing exosomes treatment attenuates acute myocardial infarction-induced myocardial damage. *Mol. Ther. Nucleic Acids* **2018**, *11*, 103–115.
[33] Zhou, Y.; Richards, A. M.; Wang, P. P. MicroRNA-221 is cardioprotective and anti-fibrotic in a rat model of myocardial infarction. *Mol. Ther. Nucleic Acids* **2019**, *17*, 185–197.
[34] K.; Serpooshan, V.; Hurtado, C.; Diez-Cuñado, M.; Zhao, M. M.; Maruyama, S.; Zhu, W. H.; Fajardo, G.; Noseda, M.; Nakamura, K. et al. Epicardial FSTL1 reconstitution regenerates the adult mammalian heart. *Nature* **2015**, *525*, 479–485.
[35] Wong, L. L.; Saw, E. L.; Lim, J. Y.; Zhou, Y.; Richards, A. M.; Wang. P. P. MicroRNA Let-7d-3p contributes to cardiac protection via targeting HMGA2. *Int. J. Mol. Sci.* **2019**, *20*, 1522.
[36] Kim, H. Y.; Bhang. S. H. Stem cell-engineered nanovesicles exert proangiogenic and neuroprotective effects. *Materials* **2021**, *14*, 1078.
[37] Mulcahy, L. A.; Pink, R. C.; Carter. D. R. F. Routes and mechanisms of extracellular vesicle uptake. *J. Extracell. Vesicles* **2014**, *3*, 24641.
[38] Jurgielewicz, B. J.; Yao, Y.; Stice. S. L. Kinetics and specificity of HEK293T extracellular vesicle uptake using imaging flow cytometry. *Nanoscale Res. Lett.* **2020**, *15*, 170.
[39] Esmaeili, A.; Alini, M.; Eslaminejad, M. B.; Hosseini. S. Engineering strategies for customizing extracellular vesicle uptake in a therapeutic context. *Stem Cell Res. Ther.* **2022**, *13*, 129.
[40] Sancho-Albero, M.; Navascués, N.; Mendoza, G.; Sebastián, V.; Arruebo, M.; Martín-Duque, P.; Santamaría. J. Exosome origin determines cell targeting and the transfer of therapeutic nanoparticles towards target cells. *J. Nanobiotechnol.* **2019**, *17*, 16.
[41] Zech, D.; Rana, S.; Büchler, M. W.; Zöller. M. Tumor-exosomes and leukocyte activation: An ambivalent crosstalk. *Cell Commun. Signal.* **2012**, *10*, 37.
[42] Caponnetto, F.; Manini, I.; Skrap, M.; Palmai-Pallag, T.; Di Loreto, C.; Beltrami, A. P.; Cesselli, D.; Ferrari. E. Size-dependent cellular uptake of exosomes. *Nanomedicine:Nanotechnol. Biol. Med.* **2017**, *13*, 1011–1020.
[43] Wang, H.; Agarwal, P.; Zhao, S. T.; Yu, J. H.; Lu, X. B.; He. X. M. A near-infrared laser-activated “nanobomb” for breaking the barriers to microRNA delivery. *Adv. Mater.* **2016**, *28*, 347–355.
[44] Xu, J. S.; Liu, Y. H.; Li, Y. J.; Wang, H.; Stewart, S.; Van der Jeught, K.; Agarwal, P.; Zhang, Y. T.; Liu, S.; Zhao, G. et al. Precise targeting of *POLR2A* as a therapeutic strategy for human triple negative breast cancer. *Nat. Nanotechnol.* **2019**, *14*, 388–397.
[45] Xu, J. S.; Liu, Y. H.; Liu, S.; Ou, W. Q.; White, A.; Stewart, S.; Tkaczuk, K. H. R.; Ellis, L. M.; Wan, J.; Lu, X. B. et al. Metformin bicarbonate-mediated efficient RNAi for precise targeting of *TP53* deficiency in colon and rectal cancers. *Nano Today* **2022**, *43*, 101406.
[46] Li, Z. H.; Wang, Z. Z.; Dinh, P. U. C.; Zhu, D. S.; Popowski, K. D.; Lutz, H.; Hu, S. Q.; Lewis, M. G.; Cook, A.; Andersen, H. et al. Cell-mimicking nanodecoys neutralize SARS-CoV-2 and mitigate lung injury in a non-human primate model of COVID-19. *Nat. Nanotechnol.* **2021**, *16*, 942–951.
[47] M.; Li, H.; Shen, D. L.; Wang, Z. S.; Liu, H. F.; Zhu, D. S.; Wang, Z. Z.; Li, L. Y.; Popowski, K. D.; Ou, C. W. et al. Decoy exosomes offer protection against chemotherapy-induced toxicity. *Adv. Sci.* **2022**, *9*, 2203505.
[48] Chen, X. R.; Zhu, L. Y.; Liu, J. Y.; Lu, Y.; Pan, L. L.; Xiao. J. J. Greasing wheels of cell-free therapies for cardiovascular diseases: Integrated devices of exosomes/exosome-like nanovectors with bioinspired materials. *Extracell. Vesicle* **2022**, *1*, 100010.